JOURNAL OF MATERIALS SCIENCE **34** (1999) 4897–4907

A study of polymer fracture surface features and their relationship to toughness

DR J. P. DEAR
Department of Mechanical Engineering, Imperial College of Science, Technology and Medicine, Exhibition Road, London SW7 2BX
E-mail: j.dear@ic.ac.uk

The aim of this study was to research fracture surface features for polymers of different toughness and type. The materials chosen provided for an interesting comparison of fracture surfaces. Two brittle amorphous thermoplastics (SAN & PMMA) of the same toughness had very different fracture surfaces. An amorphous thermoplastic (PC) exhibited similar features as both SAN and PMMA but had a higher toughness. Two semi-crystalline thermoplastics (PE1 & PE2) had similar fracture surface features but one was twice the toughness of the other. A rubber toughened polymer (ABS) showed a very different fracture surface to SAN (the host material) and all the other polymers studied. A particular interest was to use the comparison of the fracture surfaces of the above materials to investigate the toughening effects of rubber particles in ABS.

1. Introduction

Fracture processes in polymers vary greatly and this can apply to polymers that have the same toughness. Some of the factors that vary are micro-cracking about the crack tip, general and micro-yielding in the material and the drawing of fibrils across the opening crack tip [1, 2]. These and other fracture processes combine in different ways to determine the overall toughness of a material and the fracture surfaces produced. Energy absorbing fracture processes can be enhanced by the use, for example, of rubber particles [3–5]. It is difficult to define and quantify precisely the effect of these variables. However, very useful information can be obtained from a comparison of fracture surfaces of polymers of different toughness and type that have been fractured under identical conditions. This is particularly so if well defined steady state crack propagation conditions are used.

In this study, rectangular specimens of exactly the same size and shape were obtained for the following materials: styrene-acrylonitrile (SAN), polymethylmethacrylate (PMMA), polycarbonate (PC), medium-density polyethylene (PE1), high-toughness polyethylene (PE2) and acrylonitrile-butadiene-styrene (ABS). These rectangular specimens were provided with a small tongue extension, at the beginning and end of the crack path, so that the frozen tongue technique [6, 7] could be used to fracture the material. The specimens were side-grooved to minimise side-lip tearing so as to achieve, in the centre of the fracture surfaces, as near to plane strain conditions as possible. For each material, crack velocity versus applied load curves were obtained under steady state fracture conditions from the threshold load for crack propagation up to the limiting crack velocity condition. This made it possible to determine the load to achieve a crack velocity for each material that was ~70% of the limiting crack velocity. For this research, this was the crack velocity used for the study of the fracture surfaces.

The materials chosen for this study range from brittle amorphous thermoplastics to toughened multiphase ABS polymers so that different fracture surface features could be examined and related to toughness. For each material, the fracture surface was consistent for the whole length of the crack path through the specimen. SEM photographs were obtained from the centre of each crack path so as to be able to compare the difference in plane strain fracture of these materials. A problem when studying fracture surfaces using SEM techniques is that the views are two-dimensional so in this study, in addition to a plan view of the fracture surface, the specimens were sectioned so that an edge view of the fracture surface could be obtained. To achieve steady state fracture conditions and consistent crack velocities through the specimens, the frozen tongue technique [6, 7] was used.

2. Experimental

The main reasons for choosing the frozen tongue technique [6], for these studies, are as follows:

- The steady state load condition to which the specimen is subjected can be precisely defined and measured.
- Fracture can be produced in the specimens from the threshold load up to the limiting crack velocity condition for all the materials studied including the very tough ABS material. This is without using impact or other crack initiation methods that disturb

the established steady state loading conditions of the specimen.

- Crack propagation can be achieved in loaded specimens after the material has fully stress relaxed (or at different levels of stress relaxation). This is from the threshold load to just maintain the crack propagation up to the limiting crack velocity condition.
- Near to constant crack propagation conditions, for the whole length of the crack path through the specimen, can be achieved for each crack velocity.

The frozen tongue technique takes advantage of the good thermal insulation properties of polymers which permits a small tongue of material, at the beginning of the crack path, to be freeze-cooled with liquid nitrogen so that a crack can easily be initiated in the tongue with a low force device. The freezing of the tongue and the application of the crack initiation force were confined to the half of the tongue furthest from the main section of the specimen. It was verified [6] that this crack initiation procedure only caused a very small change in the stress and temperature for the first 5% of the crack path in the main section of the specimen. It was possible, in a series of experiments, each with different loading of the main section, to determine the threshold load which will just maintain crack propagation in the material and also how crack velocity varied with increasing load up to the limiting condition. Fig. 1 illustrates the frozen tongue technique including the three-point bend method for starting a sharp crack in the frozen tongue. The dimensions of the stressed main section, for the frozen tongue specimens, were width $(W) = 90$ mm, height $(H) = 180$ mm and thickness $(B) = 6$ mm. The dimensions of the tongue section of the specimen were 40 mm by 40 mm. Side grooves of depth 1 mm were used on all the specimens to provide for near to plane-strain fracture conditions. Prior to crack initiation, the main section of the frozen tongue specimen was loaded at a constant strain rate of 5 mm min^{-1} using an Instron tensile loading machine. At the required load, the machine cross-head was stopped and the specimen allowed to stress relax. After cooling of the tongue, a crack was then initiated using the three-point bend device. For each loading level of the main section, crack velocity was measured using a combination of high-speed photography and on-specimen instrumentation. For the latter, a series of conducting strips were painted onto the specimen across the line of the crack path. As these strips were broken, a staircase voltage output from an electrical circuit gave crack length versus time and hence crack velocity. This was confirmed using high-speed photography (image converter IMACON 468 camera) with backlighting so that the crack appeared as a bright streak of light passing through the specimen. The breaking of the first conducting strip triggered the camera.

Fig. 2 is a magnified close up view to show the central positioning for the sectioning of the fractured frozen tongue specimens. This is so as to obtain samples for SEM studies at near to plane strain conditions. Two views were used in this study. One was a plan view and the other an edge view from the fracture surfaces of each

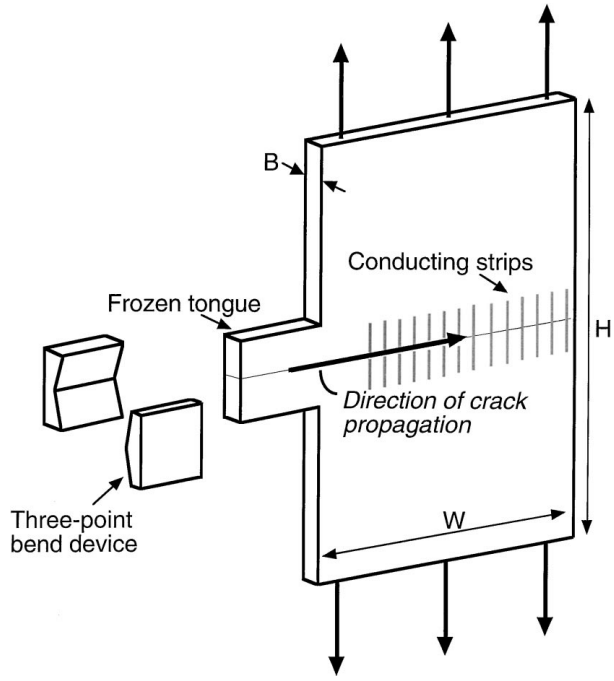

Figure 1 Frozen tongue specimen geometry. The width (W) of the main section of the specimen is 90 mm, the height (H) of the stressed main section is 180 mm and the thickness (B) is 6 mm. The tongue is 40 mm by 40 mm. The three-point bend device for crack initiation of the tongue is also shown.

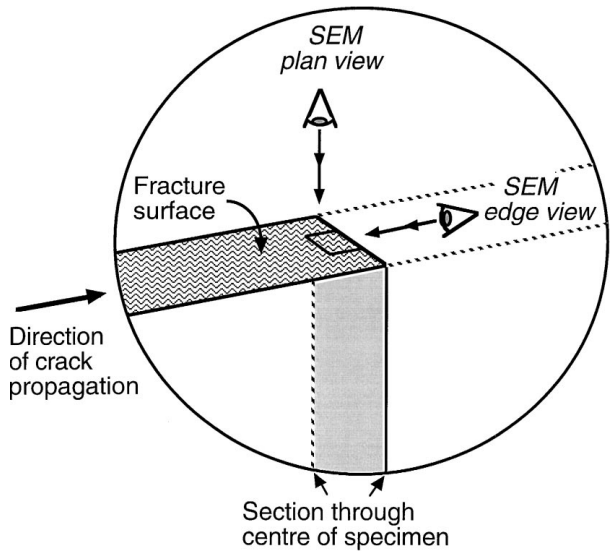

Figure 2 Magnified close up of the central part of a fractured frozen tongue specimen to show method of sectioning for obtaining samples for SEM studies. In the *plan view*, the crack runs from top to bottom of the SEM photograph and in the *edge view*, the crack advances out of the plane of the SEM photograph. For all SEM photographs (Figs 4 to 9), the magnification is 1500× and so the width of all photographs is 80 μm from the left-hand (LH) to right-hand (RH) edge.

material. In the plan view, the crack ran from top to bottom of the SEM photograph and in the edge view, the crack is advancing out of the plane of the SEM photograph (as shown in Fig. 2). In all photographs, the region of the fracture surface examined, was 80 μm from the left hand to right hand edge of the photograph (magnification 1500×). At this magnification, the well-detailed microscopic features associated with the fracture processes could be examined.

TABLE I Data for threshold load (p_0) from frozen tongue experiments, bulk value of modulus (E) from wave velocity measurements, limiting crack velocity (C_L) from frozen tongue experiments and toughness (R) from Equation 2

Material	p_0 (kN)	E (GN m^{-2})	C_L (m s^{-1})	R (kJ m^{-2})
SAN	1.6	3.3	870	0.3
PMMA	2.2	6	910	0.3
PC	2.8	3	710	1.0
PE1	3.5	1.9	570	2.5
PE2	5.5	2.3	380	5.1
ABS	8.2	2.7	490	9.1

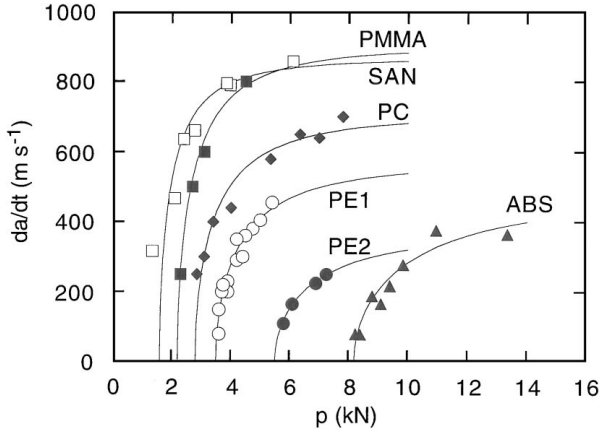

Figure 3 Crack velocity, da/dt, versus load, p, at crack initiation for frozen tongue experiments on SAN(□), PMMA(■), PC(♦), PE1(○), PE2(●) and ABS(▲). A curve (given by Equation 1) is fitted through each set of frozen tongue data to obtain values for p_0 and C_L (given in Table I).

3. Results

Fig. 3 shows the crack velocity versus load curves for the fracture of all materials studied. For each of the different materials, a curve is fitted through the plotted frozen tongue data of the form:

$$\frac{da}{dt} = C_L\left[1 - \left(\frac{p_0}{p}\right)^2\right]^{\frac{1}{2}} \tag{1}$$

where da/dt is crack velocity, p is the load, C_L is limiting crack velocity and p_0 is the threshold value of load for crack propagation. The fitting procedure provides a good measure of p_0 and C_L for each material and these values are given in Table I. The toughness, R, can be determined [7] using the relationship:

$$R = \frac{\pi p_0^2}{4EBB_NW} \tag{2}$$

where B is the overall thickness of the specimen, B_N is the crack thickness after side-grooving and W is the width of the stressed main section of the specimen. The modulus E was determined using wave velocity measurements for an excitation frequency of 2 MHz.

Figs 4 to 9 show both plan and edge SEM views of the fracture surfaces for SAN, PMMA, PC, PE1, PE2 and ABS. The crack velocities for each of these fracture surfaces examined were 800 m s^{-1} (SAN), 800 m s^{-1} (PMMA), 680 m s^{-1} (PC), 360 m s^{-1} (PE1), 250 m s^{-1} (PE2) and 380 m s^{-1} (ABS). From Table I, it can be seen that the crack velocity of the fracture surfaces studied, in each case, is ~70% of the limiting crack velocity (C_L). These SEM plan and edge views are all at the same magnification (1500×). Use of edge view SEM photographs helped to understand better the plan view SEM photographs particularly with regards to material drawn out of the plane of the fracture surface.

An advantage of using the frozen tongue technique, as described above, is that the fracture surfaces produced were very much the same texture for the whole length of the crack for all the materials studied. This is particularly so for the plane strain fracture in the centre of the specimen to which the SEM photographs relate. An interest was to study the effect, on fracture surfaces, of the presence of rubber particles in SAN material as used in ABS (The ABS material was filled with 30% by volume of rubber particles of a size 0.1–0.2 μm). Also, an objective was to compare SAN and ABS fracture surfaces with those of other polymeric materials.

Fracture processes, at the crack tip in all polymers, are many and include micro-cracking ahead of the crack tip, crazing, micro-drawing and more general yielding of the material to different extents depending upon the polymer properties. As the crack velocity approaches C_L, so there is an increasing tendency for bifurcation along the crack front. The degree and depth of upheaval of the fracture surfaces also relates to the different size of the stress-intensified zone about the crack tip. Behind the crack tip, there is rarely a clean break of the material and in some cases, there can be many fibrils bridging the crack opening surfaces. To some extent, these bridging fibrils divert the stresses away from the crack tip as does, for different reasons, the micro-cracking around the crack tip. All these fracture processes vary in degree and relate to the inherent fracture toughness properties of the material. The choice of SEM views that are shown in Figs 4 to 9 show well these differing fracture characteristics of the materials that were studied.

It is interesting that the fracture surface for SAN (Fig. 4) and for PMMA (Fig. 5) are very different although both are amorphous thermoplastics and have similar fracture toughness ($R \sim 0.3$ kJ m^{-2}). The SAN fracture surface (Fig. 4) has the appearance of a delaminating material with the laminates breaking up under shear fracture. The PMMA fracture surface (Fig. 5) is much less fragmented by crevices and other cracks but there is extensive wafer drawing of thin layers of material which then develop into fibrils.

In Fig. 6, the tougher PC material ($R \sim 1$ kJ m^{-2}) does have areas of smooth fracture surface but with more in depth cracking and peeling of thicker layers of material some of which are drawn and fractured as fibrils. It shows features similar to both SAN and PMMA in that the PC fracture surface has a layered appearance with extensive drawing of material at the edge of the layers. Also, there is breaking up of the PC fracture surface by cracks and crevices penetrating into the depth of the material.

Compared with PC, the fracture surfaces of both PE materials (PE1 ($R \sim 2.5$ kJ m^{-2}) and PE2 ($R \sim 5.1$ kJ m^{-2}) are more complicated. The plan view of

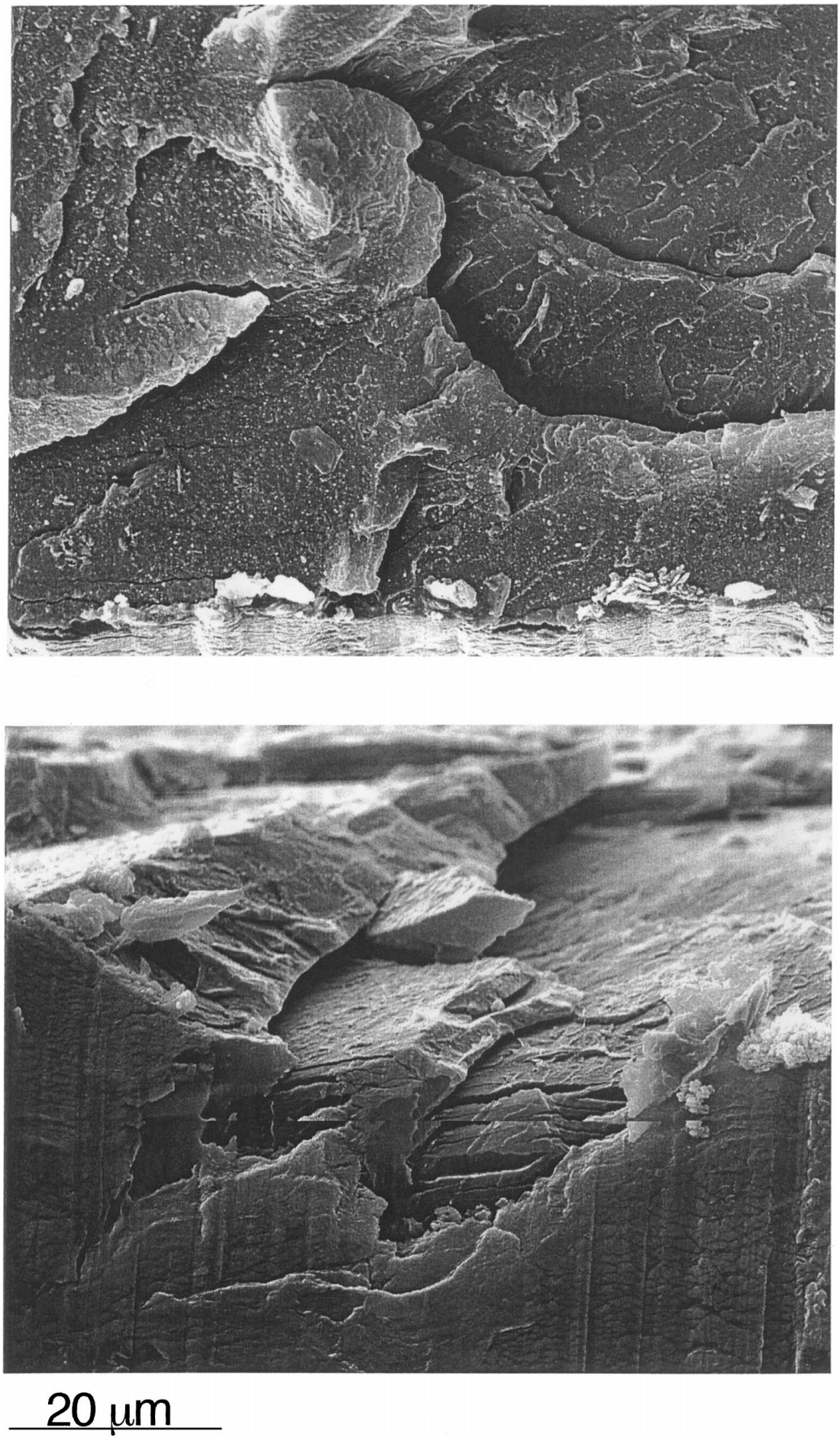

Figure 4 SEM photographs of the fracture surface of SAN (crack velocity, 800 m s^{-1}). The upper photograph is the *plan view* (crack runs from top to bottom of photograph) and the lower photograph is the *edge view* (crack advances out of the plane of the photograph). The overall width is 80 μm (from LH to RH edge).

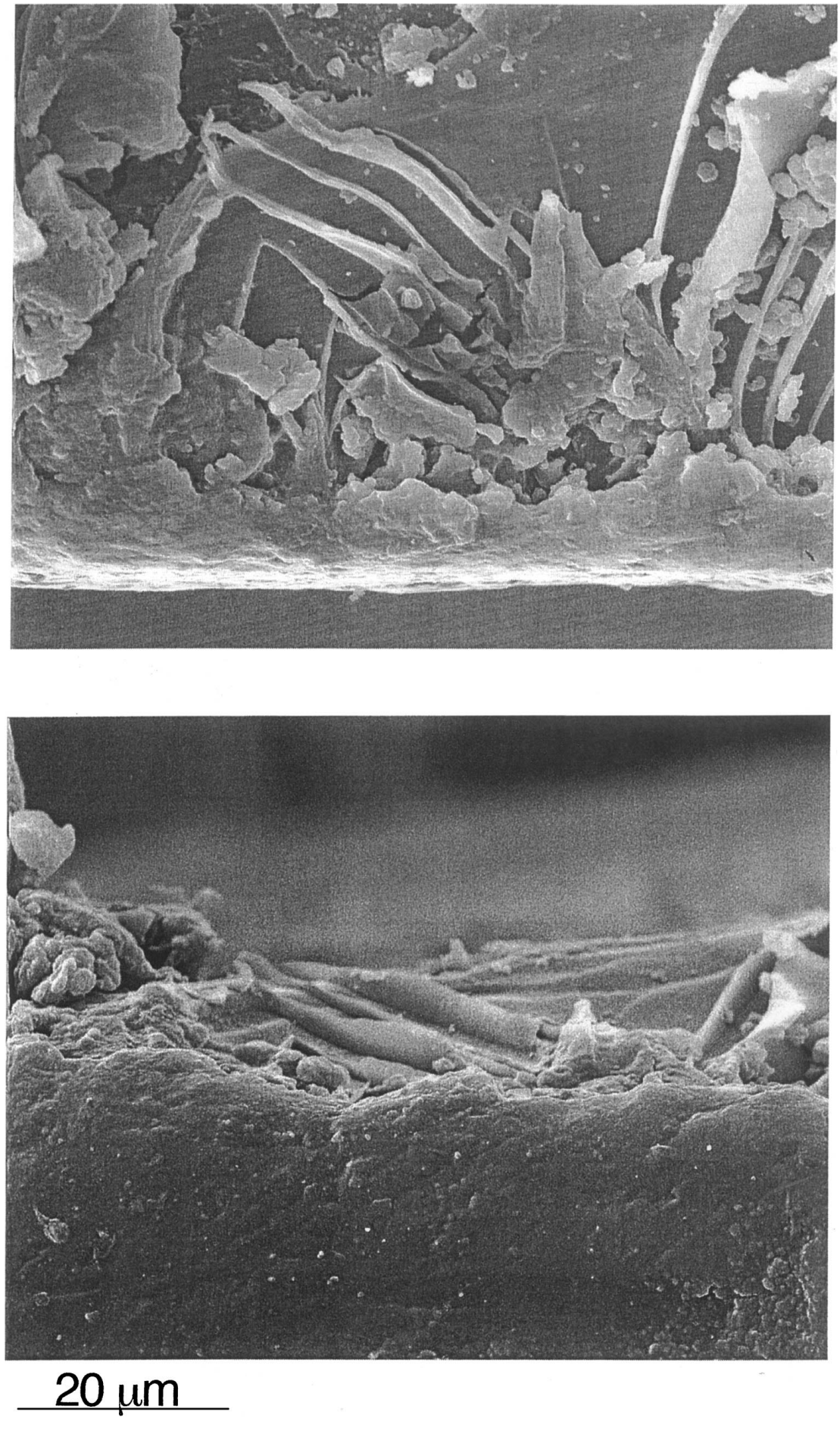

Figure 5 SEM photographs of the fracture surface of PMMA (crack velocity, 800 m s^{-1}). The upper photograph is the *plan view* (crack runs from top to bottom of photograph) and the lower photograph is the *edge view* (crack advances out of the plane of the photograph). The overall width is 80 μm (from LH to RH edge).

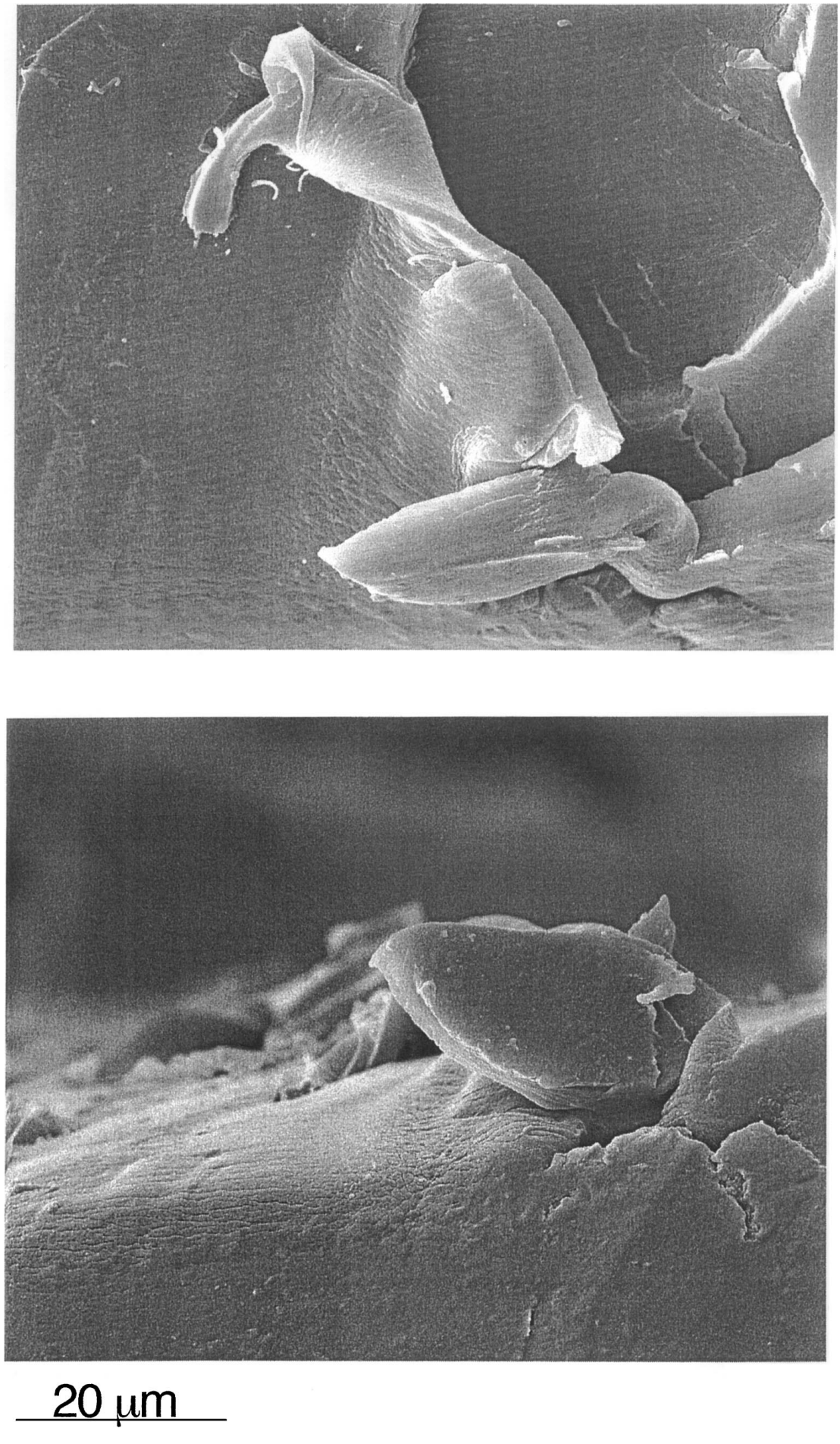

Figure 6 SEM photographs of the fracture surface of PC (crack velocity, 680 m s^{-1}). The upper photograph is the *plan view* (crack runs from top to bottom of photograph) and the lower photograph is the *edge view* (crack advances out of the plane of the photograph). The overall width is 80 μm (from LH to RH edge).

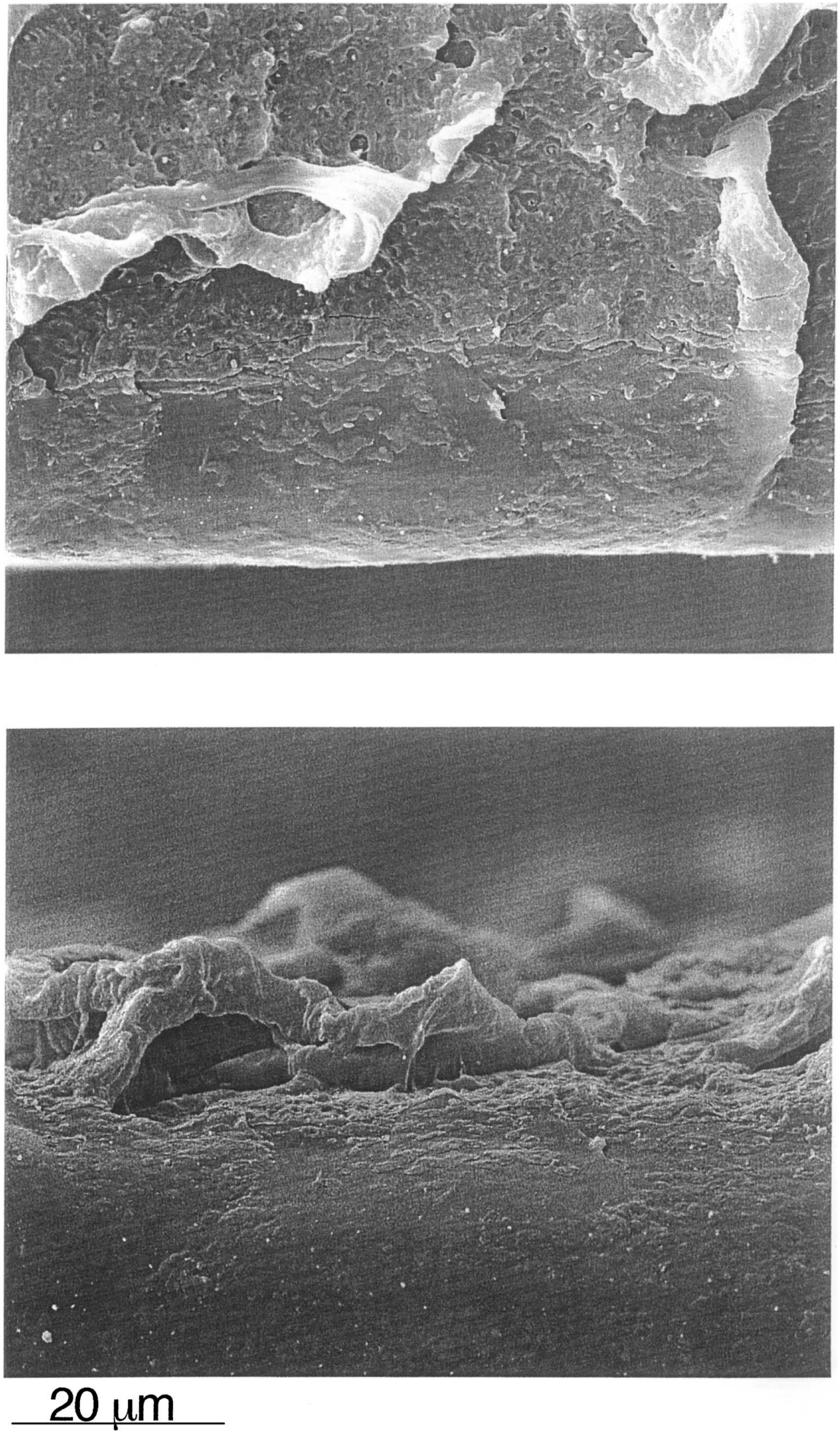

Figure 7 SEM photographs of the fracture surface of PE1 (crack velocity, 360 m s^{-1}). The upper photograph is the *plan view* (crack runs from top to bottom of photograph) and the lower photograph is the *edge view* (crack advances out of the plane of the photograph). The overall width is 80 μm (from LH to RH edge).

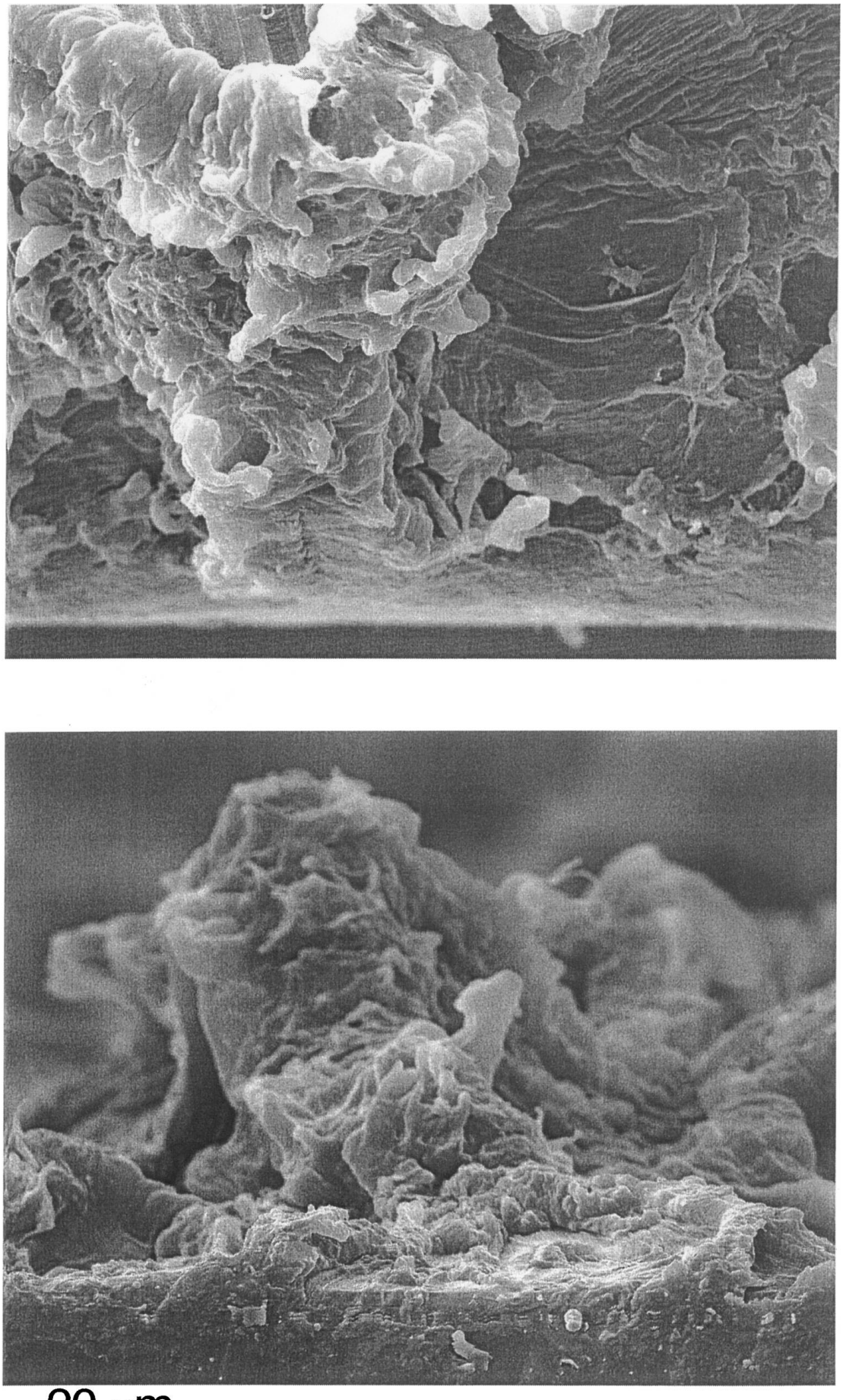

Figure 8 SEM photographs of the fracture surface of PE2 (crack velocity, 250 m s^{-1}). The upper photograph is the *plan view* (crack runs from top to bottom of photograph) and the lower photograph is the *edge view* (crack advances out of the plane of the photograph). The overall width is 80 μm (from LH to RH edge).

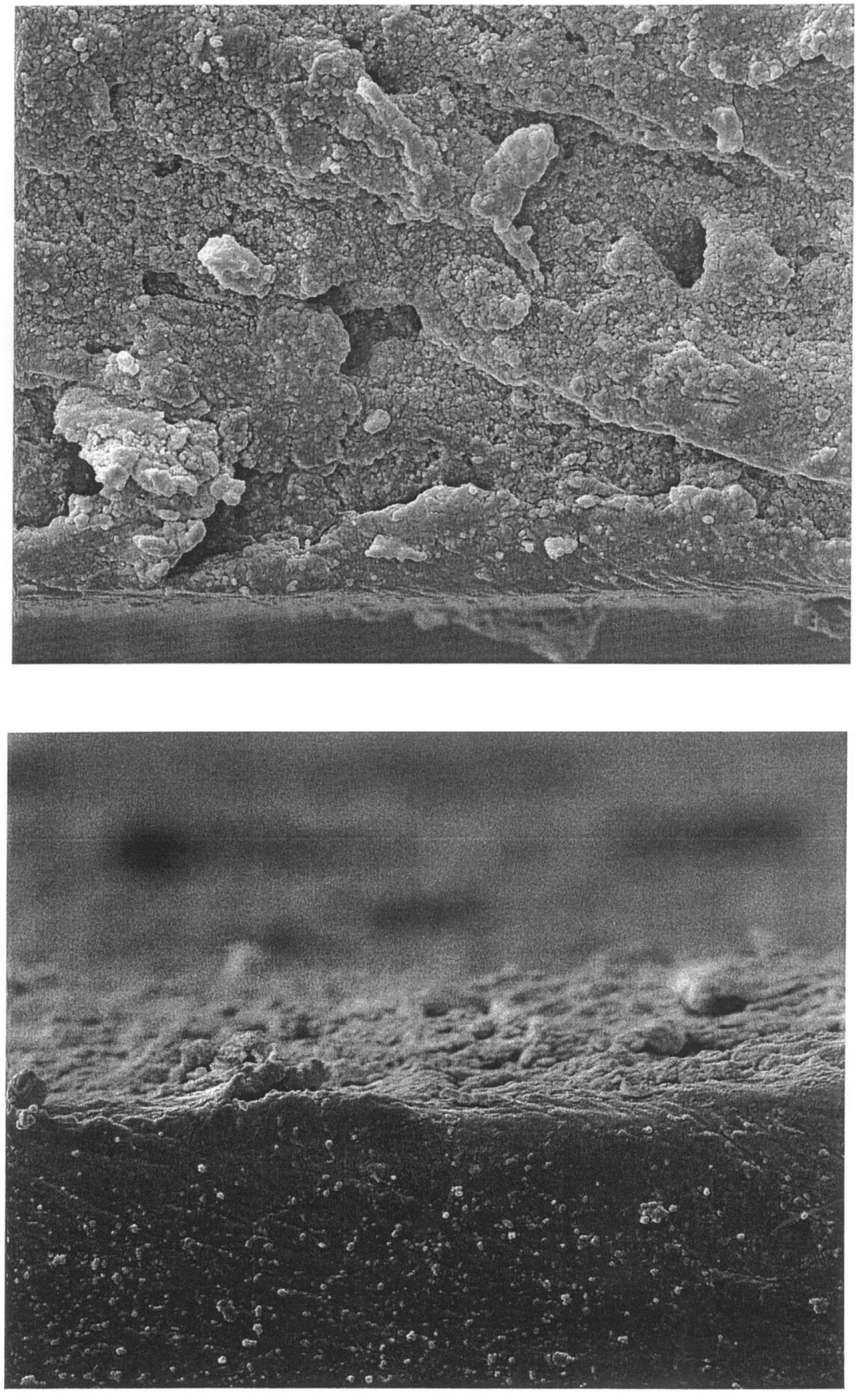

Figure 9 SEM photographs of the fracture surface of ABS (crack velocity, 380 m s^{-1}). The upper photograph is the *plan view* (crack runs from top to bottom of photograph) and the lower photograph is the *edge view* (crack advances out of the plane of the photograph). The overall width is 80 μm (from LH to RH edge).

the fracture surface of PE1 (Fig. 7) shows more drawing of material and generally has a flaky appearance. There are many thin layers of material that are drawn into wafers and then into quite long fibrils. The SEM edge view (Fig. 7) shows better the uplifting of the thin flakes of material. Much in evidence in the plan and edge view of the fracture surface of PE2 (Fig. 8) is that there is drawing of quite large plugs of material out of the plane of the fracture. These plugs of material seem to be formed by successive layers of material being drawn out of the centre of the plug and overlaid to form rosettes. Also, there is a drawing of the PE2 material in the plane of the fracture surface giving it a rippled appearance. The SEM edge view (Fig. 8) shows well the complexity of the surface of the lifted plugs of material. This difference in the fracture surfaces explains well the greater toughness of PE2 with respect to PE1.

The plan and edge views of the ABS fracture surface (Fig. 9) give the first impression of a more even and not greatly disturbed surface ($R \sim 9.1$ kJ m^{-2}). Closer inspection shows that there is an outlined profile of platelets, of the fracture surface, but these are not lifted as in the case of the SAN material (Fig. 4). In the edge view of the ABS fracture surface (Fig. 9) there is evidence of a multitude of small fracture features, which do not appear to penetrate very deeply into the ABS material. Generally, the volume of disturbed material for the ABS fracture surface is less than that of other fracture surfaces examined in this paper. However, the fracture surface of ABS is more complicated in terms of the number of features in its topology. These features are small ($\sim$1 μm in size) so there is the probability that each small feature could contain a rubber particle or have a rubber particle near to it. Crazing and shear yielding could be an important part of the failure processes of these small fracture sites. The small depth of the fracture surface could indicate that the main fracture processes occurred prior to the opening of the crack by the stress-intensified zone about and ahead of the crack tip.

The following are the main toughness features that appear in the fracture surfaces for the materials studied:

- Lifting and shear fracture of platelets,
- In plane and then out of plane drawing of material into wafers, fibrils and rosettes,
- Drawing of a plug of material out of one fracture surface by the other,
- Opening up of cavities just beneath the raised fracture surface,
- A multitude of very fine in plane and out of plane drawing of material forming little raised crowns of drawn material about depressions.

4. Discussion

A main purpose of this study was to compare fracture surfaces of polymers of different toughness with those of SAN and ABS. Of most interest was the early formation of fracture surface features and not, for example, the long drawing of fibrils by slow cracks in polyethylene. This was the main reason, in this study, for fracturing specimens at a crack velocity of $\sim$70% of each material's limiting crack velocity. An important requirement was that the fracture surface features should be consistently repeated along the whole length of the fracture path and be related only to the inherent properties of the material. To be avoided were features that related to transient vibration of the specimens, boundary reflections and other unwanted disturbances of this kind so as to achieve steady state fracture conditions. This was the reason for using the frozen tongue technique which also provided for precise measurement of the strain energy available to the crack tip, after the specimens had been loaded and allowed to stress relax in a fixed grip arrangement, prior to crack initiation.

The frozen tongue specimens used were conveniently small for laboratory experiments but of dimensions to provide for on-specimen instrumentation to measure crack velocity and to monitor stress intensity at the crack tip. Determining the required crack velocity ($\sim$70% of the limiting crack velocity for each material) was achieved by plotting crack velocity versus load curves for each material from the threshold load to just maintain crack propagation up to the limiting crack velocity condition (see Fig. 3).

Often, the first phase of the generation of fracture surfaces is the formation of micro-cracks and other damage by the stress-intensified zone ahead and about the propagating crack tip. These micro-cracks can coalesce into larger cracks and voids prior to the opening of the crack tip. Depending upon the size of the crack tip stress-intensified zone and the physical properties of the material, this micro-cracking damage can be considerable. This can add to the tendency of different parts of the crack front to deviate above and below the main crack path (bifurcation) as the crack front seeks out weak paths through the disturbed material ahead of its tip.

It is notable that the use of rubber particles to toughen the brittle SAN host material is very effective and achieves an ABS material of high toughness. The fracture toughness of PMMA and SAN are similar but their fracture surfaces are very different. For PMMA, there are thin platelets of material where the lifted edges have been drawn into wafers and fibrils as the crack opens. For SAN, the lifted platelets of material are thicker and appear to have undergone shear fracture giving the surface the appearance of material being delaminated at several levels. The fracture surface of PC exhibits features found in SAN and PMMA. For these three materials, their fracture surface features are thought to relate closely to the degree of micro-cracking ahead and about the crack tip. In the case of PE1, there is more general yielding of the surface material with plugs of material being drawn out of one surface by the other. Often, open cavities are formed in the side or under the raised plugs of material. Also, well in evidence, particularly in the PE2 fracture surface, is an extensive number of small sites of material drawn in and out of the plane of the fracture surface giving the material a very rough contoured appearance with spikes, rosettes and similar features.

It is very interesting that the ABS fracture surfaces do not have drawn material in the form of large plugs, wafers and fibrils and the fracture surfaces are generally quite flat. However, there are a large multitude of very small sites of deformation ($\sim$1 μm in size) which could contain a rubber particle or be near to one (see Fig. 9). Each of these small sites could have failed due to crazing or shear yielding. It is possible that many of these small sites fractured before the final opening of the crack and other sites failed as soon as the crack started to open. It is interesting to note that ABS and SAN have very much the same linear stress-strain curve up to a point when the SAN fails at impact loading rates. After this failure point in the SAN, the ABS stress-strain curve continues but is non-linear. This suggests rubber particles are able to restrict crack growth by promoting crazing or shear yielding about the rubber particles and this is particularly effective in brittle host materials like SAN.

A summary of the main features of the ABS fracture surfaces compared with those of other materials studied is as follows:

- The ABS fracture surface has shallow steps, which appear to relate to the boundary of platelets, similar to those in the SAN fracture surface. However, the platelets in ABS are not lifted and remain integrated with the main fracture surface. Hence, there is no shear fracture of the platelets as in the case of the SAN material.
- There is no evidence in the ABS fracture surface of large wafers, fibrils and lifting of plugs of material as seen in PMMA, PC, PE1 and PE2 fracture surfaces.
- Crevices, cavities and other induced faults, penetrating into the depth of the ABS fracture surface, are small and have a blunted appearance.
- Generally, all the ABS fracture surface features seem to be confined to a relatively thin layer of disturbed material.
- A notable feature of the ABS fracture surface is the presence of a multitude of tiny fracture sites (1 μm in size) consisting of raised material with a pit or rosette at their centre. These are not evident in the SAN fracture surface. Each tiny fracture site, in the ABS, could have a rubber particle or be near one. These rubber particles can promote energy-absorbing crazing, shear yielding and similar processes in and about the small sites and so make a major contribution to the toughness of ABS. It is possible if rubber particles are immediately in the crack path, they can be drawn as the crack opens and bridge the crack tip.
- About the rubber particles, triaxial stresses can be generated which promote crazing and shear yielding. In this process, the rubber particles can deform, cavitate and absorb energy in other ways. Generally, the presence of the rubber particles resists the opening of the crack tip as part of increasing the toughness of the material.

5. Conclusions

Fracture surfaces of the materials studied reveal there can be a propensity for flakes or layers of material to form which could relate to the micro-cracking ahead of the crack tip. This is particularly so in the materials studied which did not have rubber toughening. In some cases, the layers tend to be thick and then fracture in shear. In other cases, the platelets are very thin and the edges of the platelets peel back to produce wafers and fibrils. A different feature is for a layer to be pulled together into a plug of material. Often, under these plugs of material, there are open cavities. In the formation of these features, much depends upon the inherent properties of these materials particularly with regards to the tendency for the material to yield. In brittle materials, there is a greater tendency for crevices and cracks to be generated normal to the crack path.

Very interesting is the ability of small rubber particles in ABS to restrict cracking by crazing or shear yielding of the brittle SAN host material. This includes limiting the growth of micro-cracks ahead of the crack tip. Also, in ABS the lifting of the platelets seems to be inhibited or restricted. The result is that the ABS fracture surface appears to have less depth of disturbed material than the other polymers studied. An important toughening feature in ABS seems to be the generation, about the rubber particles, of a multitude of very small fracture sites. The indication is that some of these sites fail prior to the opening of the crack and others as soon as the crack starts to open. This would account for the fracture surface having overall a flat appearance.

Acknowledgements

The author thanks the Engineering and Physical Sciences Research Council (EPSRC) and the Polymer Engineering Group (PEG) for their valuable help and support.

References

1. H. SCHARDIN, in "Fracture" edited by B. L. Averbach, D. J. K. Fellbeck, G. T. Hahn and D. A. Thomas (Wiley, New York, 1959) chap. 16.
2. C. S. LEE and M. M. EPSTEIN, *Polymer Engng. & Sci*. **22** (1982) 9.
3. C. B. BUCKNALL and R. R. SMITH, *Polymer* **6** (1965) 437.
4. C. B. BUCKNALL, *Advances in Polymer Science* **27** (1978) 121.
5. A. M. DONALD and E. J. KRAMER, *J. Mater. Sci*. **17** (1982) 1765.
6. J. P. DEAR, *ibid.* **26** (1991) 321.
7. J. P. DEAR and J. G. WILLIAMS, *ibid.* **28** (1993) 259.

Received 12 February
and accepted 19 March 1999